Journal of Electroanalytical Chemistry 707 (2013) 156–165

Contents lists available at ScienceDirect

Journal of Electroanalytical Chemistry

journal homepage: www.elsevier.com/locate/jelechem

A detailed look at electrical equivalents of uniform electrochemical diffusion using nonuniform resistance–capacitance ladders

Yannis Tsividis [a,1], John Milios [b,*]

[a] Department of Electrical Engineering, Columbia University, New York, NY 10027, USA
[b] Sendyne Corp, 250 West Broadway, New York, NY 10013, USA

ARTICLE INFO

Article history:
Received 2 April 2013
Received in revised form 13 August 2013
Accepted 20 August 2013
Available online 28 August 2013

Keywords:
Diffusion
Battery modeling
Equivalent circuits
Warburg impedance
Electrochemical impedance

ABSTRACT

This paper discusses equivalent-circuit modeling of the electrochemical impedance corresponding to one-dimensional diffusion in a uniform medium. It argues that, of the several equivalent circuits in use for such modeling, one – namely the nonuniform resistance–capacitance ladder – has attractive properties that are not shared by any other equivalent circuit. Explicit, analytical expressions are derived for the efficient development of this ladder equivalent, which provide advantages compared to computer optimization. Although the context of this work is battery modeling, the results presented can be of value in other fields where diffusion is studied and modeled.

1. Introduction

The modeling of the electrochemical impedance corresponding to one-dimensional diffusion in a uniform medium [1–7] using electrical circuit analogs has been discussed extensively in the literature [2–5,7–20]. A significant number of alternative equivalent circuits has been presented for this purpose, including Voight (Foster) circuits, Maxwell circuits, and equal-*R*, equal-*C* ladder structures [9,20]. This paper argues that nonuniform ladder equivalents have certain unique properties not shared by other circuits. In contrast to the common practice of determining the element values of such circuits by computer optimization [21,22], this paper develops analytical methods for doing so, and discusses several advantages that can be had by using such an approach. These include the ability to model internal time-domain behavior (as opposed to only external frequency-domain behavior represented by the electrochemical impedance), predictive capability, and efficient computation. These and other advantages, discussed later in this section, make the model suitable for an important emerging application: the computer simulation of mixed electrochemical/electrical systems, such as systems involving both energy storage devices and power electronics. The need for efficient simulation of such systems arises during their design, as well as in their deployment in the field, where on-site, real-time computation can be an important aid in maximizing the performance of the energy storage devices involved. The attributes of the model presented make it attractive for inclusion in more extensive models, containing additional elements that model phenomena not addressed in this paper.

In order to prepare for the arguments to be made in this paper, we consider the diffusion-electrical circuit correspondence, shown in Fig. 1, in some detail. Diffusion is assumed within the structure of Fig. 1a, with volume density $\rho(x,t)$ and flux (number of particles per unit of cross-sectional area, per unit time) $j(x,t)$, where x is position and t is time. This structure is characterized by the continuity equation:

$$\frac{\partial \rho}{\partial t} = -\frac{\partial j}{\partial x} \tag{1}$$

Assuming a constant diffusion coefficient D, Fick's first law is:

$$j = -D\frac{\partial \rho}{\partial x} \tag{2}$$

Inserting (2) into (1) we obtain Fick's second law (the "diffusion equation"):

$$\frac{\partial \rho}{\vartheta t} = D\frac{\vartheta^2 \rho}{\vartheta x^2} \tag{3}$$

* Corresponding author.
E-mail address: jmilios@sendyne.com (J. Milios).
[1] This work was performed for Sendyne Corp.

1572-6657
http://dx.doi.org/10.1016/j.jelechem.2013.08.017

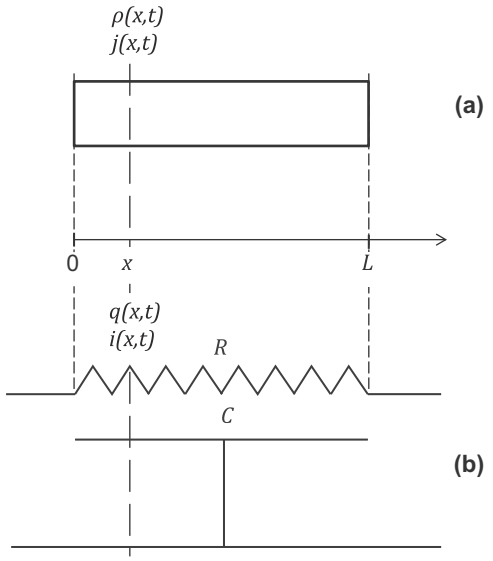

Fig. 1. (a) One-dimensional diffusion and (b) corresponding one-dimensional distributed *RC* circuit. The structures have the same length, *L*.

The structure in Fig. 1b is a linear uniformly-distributed *RC* structure of the same length *L* as the top structure, characterized by total resistance *R* and total capacitance *C*, corresponding to resistance per unit length $r = R/L$ and capacitance per unit length $c = C/L$, respectively. The current at position *x* is denoted by $i(x,t)$, and the charge per unit length stored at position *x* is denoted by $q(x,t)$. Fig. 2 shows corresponding incremental elements of the structures in Fig. 1. In Fig. 2b, the net increase in the charge in time Δt is $i\Delta t - (i+\Delta i)\Delta t = -\Delta i\Delta t$, which corresponds to a charge increase per unit length of $\Delta q = -\Delta i\Delta t/\Delta x$. Allowing finite differences to approach 0, we obtain:

$$\frac{\partial q}{\partial t} = -\frac{\partial i}{\partial x} \tag{4}$$

From Ohm's law we have $i = -\Delta v/(r\Delta x)$; the changes in v and q over the length Δx are related by $\Delta v = \Delta q/c$. Combining these two equations we obtain $i = -\Delta q/(rc\Delta x)$. Allowing finite differences to approach 0, we obtain:

$$i = -\frac{1}{rc}\frac{\partial q}{\partial x} \tag{5}$$

Inserting (5) into (4) we obtain:

$$\frac{\partial q}{\vartheta t} = \frac{1}{rc}\frac{\vartheta^2 q}{\vartheta x^2} \tag{6}$$

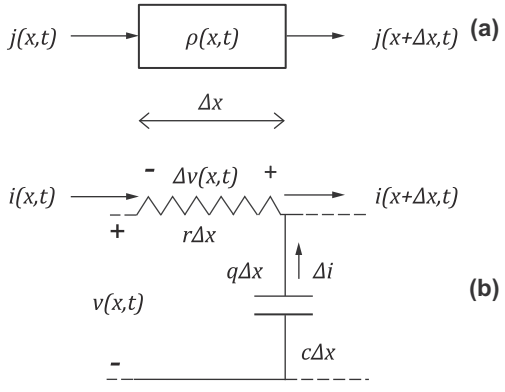

Fig. 2. Incremental elements of the structures in Fig. 1.

Table 1
Correspondence between quantities in diffusion problem and in electrical analog.

Diffusion problem – Fig. 1a	Electrical analog – Fig. 1b
Volume density, ρ	Charge per unit length, q
Diffusion flux, j	Electric current, i
Diffusion coefficient, D	$1/rc$

The correspondence of the two structures in Fig. 1 is now apparent, with (4)–(6) corresponding to (1)–(3) respectively, if the analogies shown in Table 1 are made.

For the structure in Fig. 1b, the equation for the current, $i(x,t)$, has the same form as (6), with q replaced by i [23], and the voltage can be found from:

$$v = \frac{q}{c} \tag{7}$$

The correspondence of physical variables in Table 1 is not only qualitative, but also quantitative. Thus, the charge in the structure of Fig. 1b is numerically equal to the volume density in Fig. 1a, at the same position and the same time, if one chooses $1/rc = D$ and analogous excitation. Thus the analogy does not only hold for the external behavior across, say, the port on the left, but rather holds throughout the structure. This detailed analogy can be crucial, as discussed below.

1.1. Need for equivalent circuits

Electrical equivalent circuits for the structure of Fig. 1a have been used for a long time. Such circuits allow for efficient computer simulation of this structure by highly-developed electrical circuit simulators, such as Spice [24,25], not only for the small-signal electrochemical impedance (which, after all, could also be computed analytically), but also for transient response to a variety of excitations.

In recent years, another reason for using electrical equivalents has emerged. Electrochemical devices, such as batteries and supercapacitors, are increasingly incorporated into sophisticated electronic systems. The resulting hybrid (electrochemical/electronic) systems need to be analyzed as a whole; for example, a designer of power conversion circuits needs to analyze complicated circuits that interface directly with a battery. In order to be able to use circuit analysis computer aids, such as Spice, for the simulation of the hybrid systems mentioned above, one needs to model batteries and supercapacitors in terms of equivalent electrical circuits. Such equivalent circuits, besides modeling other phenomena [3,9–13], need also to include structures such as the one shown in Fig. 1b to model diffusion.

Most circuit simulators have been developed for lumped-element circuits described by nodal equations, and have difficulties handling distributed elements, for which nodal equations cannot, in principle, be written. In various versions of the popular Spice simulator, one may consider using the available transmission-line elements, with an appropriate definition of their parameters, to model a distributed structure. However, such use is plagued by numerical issues; for example, calculating the real part of electrochemical impedance at very low frequencies can result in very large errors (and even result in negative values). Transmission line models are also known to have numerical problems in transient simulations, which are essential in some electrochemical device work (e.g., battery system simulation). Finally, known transmission line models in circuit simulators are inherently linear elements, and one cannot introduce nonlinearities in them.

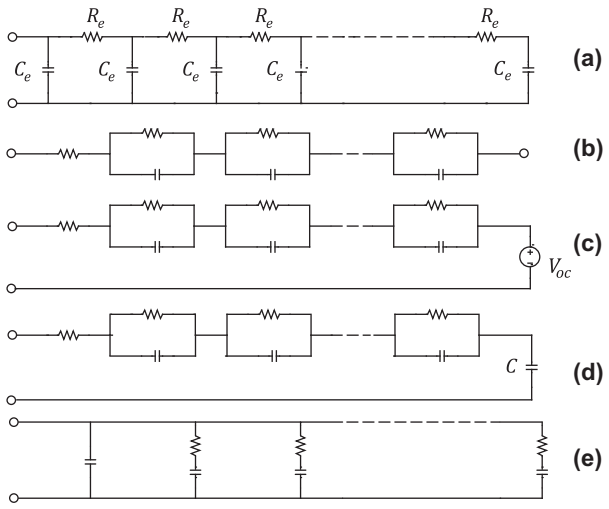

Fig. 3. Alternative circuits for modeling electrochemical impedance. (a) Equal-*R*, equal-*C* ladder; (b) Voight or Foster circuit; (c) the circuit in (b) in series with a voltage source representing the open-circuit voltage of a battery; (d) the circuit in (b) in series with a capacitance representing storage; (e) Maxwell circuit (or Foster admittance realization circuit).

1.2. Popular equivalent electrical circuits

The most straight-forward lumped-element representation of the distributed structure in Fig. 1b is called the ladder circuit, and it is shown in Fig. 3a. The total resistance and total capacitance of the structure is split into a large number of equal resistances and capacitances as shown [9,20]. As will be seen, though, for adequate modeling one needs a huge number of *RC* sections. Thus, several other circuits are used instead for representing electrochemical impedance [7,15,16,18,19]. It is known that different internal circuit topologies can exhibit the same impedance across their two external terminals [26], so it is not surprising that several different circuits have been used for electrochemical impedance modeling. The circuit in Fig. 3b is called the Voight circuit in [15], but is known as the Foster circuit in electrical network theory [26]. This equivalent circuit has been used to model systems exhibiting a variation of properties along geometrical dimensions, and the associated distribution of time constants [27]. However, if this circuit is used to model electrochemical impedance, it clearly can do so only at sufficiently high frequencies; at very low frequencies, where the capacitances can be viewed as open circuits, this circuit reduces to just a resistance, failing to model storage, in contrast to the ladder in Fig. 1a, which reduces to a capacitance at such low frequencies. The circuit of Fig. 3b is sometimes used in conjunction with a voltage source representing the open-circuit voltage of a battery, as shown in Fig. 3c. For an ideal voltage source, this circuit exhibits identical AC impedance as the one in Fig. 3b, and thus fails to represent storage. This can be attempted to be rectified by using a capacitance *C* in place of the voltage source, as shown in Fig. 3d. At very low frequencies, this capacitance is all that is seen across the terminals, and in order to match the storage behavior, it must be equal to the total storage capacitance. This means that the rest of the capacitances do not have clear physical meaning related to storage, but nevertheless they are needed in order to represent the correct AC external impedance. Finally, Fig. 3e shows a so-called "Maxwell" structure, known in electrical circuit theory as a Foster admittance realization [26]. At very low frequencies, the capacitance seen across the terminals of this structure is the sum of the individual capacitances – a property shared by the ladder circuit.

The circuits in Fig. 3b–e share a common problem. Unlike the ladder in Fig. 3a, the individual nodes in those circuits do not correspond to internal points in the diffusion problem in Fig. 1a. To see this, consider an application of an external excitation across the terminals of any of these circuits. In circuits (b)–(d), it follows from Kirchhoff's current law that the current entering each parallel *RC* circuit is equal to the current leaving it, and equal to the input current. Thus as soon as the input current is applied, all nodes in these circuits are activated simultaneously, and this is communicated to all node voltages; there is no notion of *internal* delay in these circuits. In the circuit of Fig. 3e, a similar observation can be made: all voltages across the vertical branches are equal to the terminal voltage, and thus all change instantaneously, as soon as the input voltage changes; no propagation of the input disturbance is evident from left to right (for that, one would have to look at the individual capacitor voltages, but the correspondence of those to the situation of Fig. 1a is far less obvious). In contrast to this, the ladder circuit in Fig. 3a maintains a close correspondence to that of Fig. 1b, which in turn represents exactly the diffusion problem illustrated in Fig. 1a.

The above observations make the difference between the ladder in Fig. 3a and the models in Fig. 3b–e clear: The latter are circuits meant to model the *external* behavior of the distributed structure in Fig. 1b, but they are not useful for representing the internal behavior of the structure. For example, the circuit in Fig. 3d can have the same mathematics as far as the impedance observed *externally* is concerned, but different mathematics internally.

The ladder in Fig. 3a, by contrast, can model both the *external* and the *internal* behavior of the distributed structures of Fig. 1. As a consequence, the transient behavior of the distributed structure can be studied by imposing initial charges on the capacitors in Fig. 3a (corresponding to initial volume densities in the structure of Fig. 1a), and then simulating with an electrical simulator; this is not possible for the rest of the structures in the in Fig. 3.

The close analogy of the physics of the electrochemical and ladder structures becomes even more important if other effects are considered, such as nonlinearities, which are now briefly discussed. In the development leading to (3), we have assumed that the diffusion coefficient is constant. In the more general case, the diffusion coefficient can be a function of the density and/or other factors, leading to a nonlinear diffusion equation; this can be modeled if the resistors and capacitors in the ladder are allowed to be nonlinear. This fact, and the capabilities and properties of the resulting structure, are part of an extensive study that will be reported separately.

1.3. Need for a nonuniform RC ladder equivalent circuit

Having discussed the advantages of the *RC* ladder equivalent circuit in Fig. 3a, we now return to its major disadvantage, which has already been mentioned above: In order for this structure to give acceptable results, a huge number of *RC* sections must be used. For example, one needs over 5000 sections in order to model the impedance phase within a 0.5° error, in the constant phase region over a frequency range of 3 decades (Section 4). This makes the structure unsuitable for practical purposes. This drawback can be traced to the use of equal-*R*, equal-*C* elements. If unequal-*R* and unequal-*C* elements are allowed, as indicated in Fig. 4, much more

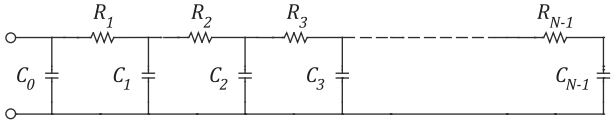

Fig. 4. Nonuniform *RC* ladder representation of the distributed structures of Fig. 1. This representation is studied analytically in this paper.

efficient modeling is possible. This has been proven using computer optimization of such ladders [21,22,28].

Computer optimization though, however valuable it may be, is not a substitute for analytical results. There are several reasons for this: (a) Computer optimization is, as far as the user is concerned, a blind process; it does not provide insight into the workings of the system being optimized, in contrast to analytical results. (b) Computer optimization is useful for matching computed results to available data; it cannot be used to predict behavior before such data is available, in contrast again to analytical results. (c) Computer optimization can be a time-consuming process; in fact, it can fail for high-order systems, unless a very good first guess is provided. These issues can become critical in cases where rapid computation is needed, as is the case, for example, in sophisticated battery management systems, where a resident model must be dynamically adapted to predict the behavior for different values of the state of the battery. It is not just impractical to have to run an optimizer each time such updates are needed; it is actually impossible, as no data are available to be matched for such updates. In fact, the main reason for the existence of models in such applications is to *predict* behavior in the absence of appropriate data.

For the above reasons, the rest of this paper derives analytical results for the nonuniform structure of Fig. 4 with emphasis on high accuracy and computational efficiency. The finite-length, blocking-boundary electrochemical impedance will be used as a vehicle to illustrate the principles, which themselves are of general validity.

A promising direction toward developing an efficient nonuniform ladder representation will now be discussed with the help of Fig. 5, which shows part of a distributed structure to be modeled. The right end of the structure (not shown) is assumed to be open-circuited. We seek to model the input impedance at the input port, indicated on the left with an arrow. One may intuitively expect that attention must be paid to modeling more accurately the parts of the structure that are near the input port, as those affect the input impedance directly. On the other hand, the further away segments of the structure are from that port, the less accurately they need to be modeled, since their effect is seen at the input only indirectly, through other segments. One may thus attempt to divide the structure into progressively longer segments, as those shown bounded by the broken lines in Fig. 5, and use a lumped representation for each segment. This observation naturally leads to a ladder representation of the type shown in Fig. 4, where it can now be expected that the capacitance and resistance values will be progressively larger toward the right. While these observations are only intuitive at this point, they will be seen to be confirmed by the results of the mathematical development that follows. It is noted that the use of a nonuniform ladder as in Fig. 4 in no way implies that the diffusion being modeled is nonuniform; we remind the reader that the diffusion coefficient is assumed to be constant, independent of position, as has been stated above (2). In fact, the entire purpose of this paper is to efficiently model uniform diffusion using analytically-determined nonuniform ladders, and to discuss the several advantages that ensue.

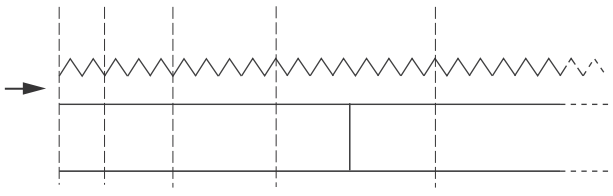

Fig. 5. Uniform distributed *RC* structure, separated into progressively longer segments, each to be modeled by a lumped approximation, for the purposes of modeling the input impedance on the left. The right end of the structure (not shown) is assumed to be open-circuited.

2. Finite-length, blocking-boundary electrochemical impedance

In this paper we will use the term "electrochemical impedance" rather than "Warburg impedance". The latter term is normally used in the original context of [1], in which diffusion over infinite length is considered. The more realistic case of diffusion over a finite length has been treated extensively in the literature [2–7], and the associated impedance is sometimes referred to as "finite-length Warburg impedance". This impedance depends on the boundary conditions. In this work we concentrate on a finite-length structure with a blocking boundary, i.e. with diffusion prevented at the right end as shown in Fig. 1a [3,4]; this will be seen to be of special use in battery modeling, which is the context in which this work has originated. This situation corresponds to the structure of Fig. 1b, with finite length L, and with a boundary condition imposed by an open circuit at its end, i.e. $i(L,t)=0$. The voltage and current equations can be solved to provide the corresponding Laplace transforms $V(x,s)$ and $I(x,s)$, where s is the Laplace transform variable [26]. One can then solve for the resulting $V(x,s)$ and $I(x,s)$ and use them to calculate the input impedance of the structure:

$$Z_o(s) \equiv \frac{V(0,s)}{I(0,s)} \tag{8}$$

which can be shown to give [23,29]

$$Z_o(s) = \frac{R}{\sqrt{sRC}} \coth \sqrt{sRC} \tag{9}$$

where R and C are respectively the total resistance and capacitance of the line. The quantity $Z_o(s)$ is the blocking-boundary, finite-length diffusion impedance. It is of the same form as the one derived directly for the corresponding electrochemical systems [2–5].

To determine the frequency response, we use in (9):

$$s = j\omega = j2\pi f \tag{10}$$

with ω the radian frequency in rad/s and f the frequency in Hz. The phase and magnitude of $Z_o(j\omega)$ are shown in Fig. 6a and b, respectively. Three regions can be identified on the phase plot: A region where the phase is essentially $-90°$, thus corresponding to (capacitive) storage; a region where the phase is essentially $-45°$, thus corresponding to the behavior of a constant-phase element (CPE); and a transition region between the two, which includes a point at which the phase peaks (for future reference, we note that this point is at $fRC = 1.224$). The exact boundary positions between regions depend on the phase error one is willing to accept for the two outer regions.

Phase and magnitude plots are more valuable than Nyquist plots for our purposes; in the latter, small phase errors are difficult to spot, and the parametric representation used in them makes it difficult to compare two superimposed plots. As phase and magnitude plots do not have this problem, they were selected for use in this paper.

It is not easy to distinguish the boundaries between regions in the magnitude plot, shown in Fig. 6b. Thus, in this paper we will emphasize phase plots, which provide a more sensitive indication of the accuracy of the approximations we are about to introduce.

For future reference, we note that, from (9) and (10), the following holds:

$$\lim_{\omega\to\infty} Z_o(j\omega) = 0 \tag{11}$$

As already mentioned, the impedance in (9) is different from what is commonly called "Warburg impedance" [1], which characterizes structures of infinite length, and results in $1/\sqrt{s}$

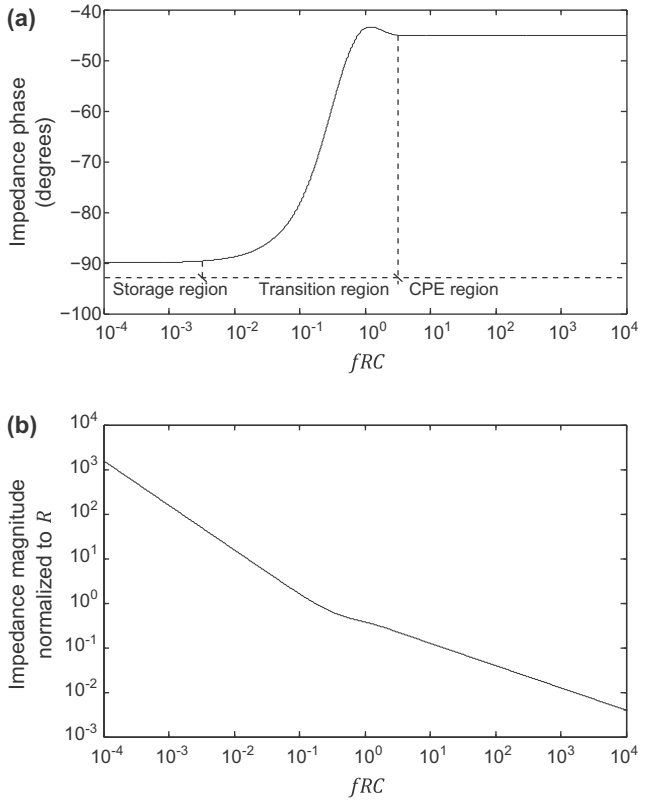

Fig. 6. (a) Phase and (b) magnitude of impedance of the distributed structure of Fig. 1b, as a function of *fRC*.

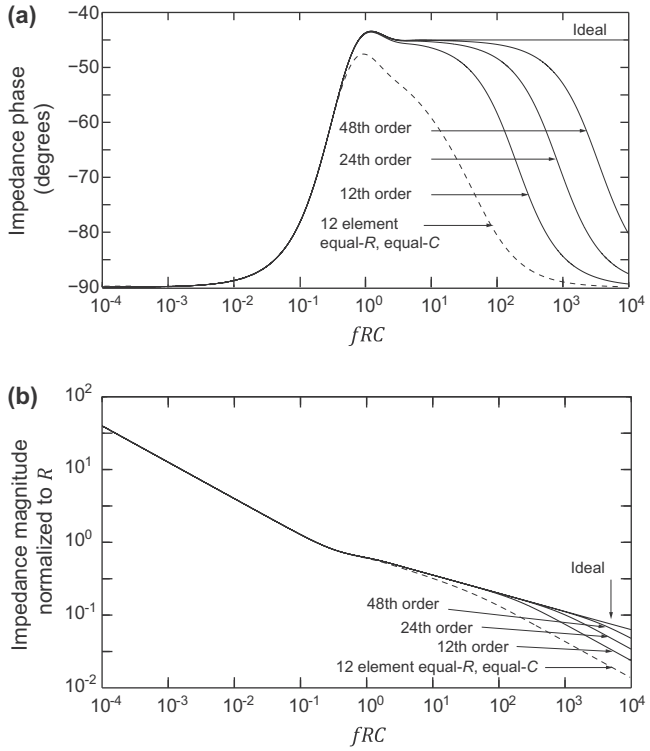

Fig. 7. Solid lines: Truncated Weierstrass approximation compared to ideal (distributed structure) impedance as a function of *fRC*, for different orders of approximation. Broken lines: Corresponding results from a 12th order equal-*R*, equal-*C* ladder. (a) Phase and (b) magnitude.

dependence, but without the coth factor seen in (9). Equivalent circuits for the (infinite-length) Warburg impedance often model the CPE behavior only [19]. Such models cannot capture the behavior of the transition region from low- to high-frequency behavior; yet this transition region turns out to contain important diagnostic and identification information [6,30].

The above exact results can be used to illustrate the failure of the equal-*R*, equal-*C* ladder, which has already been mentioned. Such a ladder, with 12 capacitors, gives the impedance shown by the broken lines in Fig. 7 (the rest of the lines will be discussed below); it is seen that this approximation fails in both the transition and CPE regions.

2.1. Rational expression based on Weierstrass product expansions

The impedance in (9) cannot be represented by lumped-parameter electrical circuits, as such circuits have rational transfer functions. In order to be able to employ such circuits, an approximation of (9) using rational transfer functions becomes necessary [23,29,31]. This equation can be written as:

$$Z_o(s) = \frac{R}{\sqrt{sRC}} \frac{\cosh\sqrt{sRC}}{\sinh\sqrt{sRC}} \tag{12}$$

We now find the roots of the numerator and denominator of the second fraction in this equation. Using

$$\theta \equiv \sqrt{sRC} \tag{13}$$

we set $\cosh\theta = (e^{\theta} + e^{-\theta})/2 = 0$, from which $e^{2\theta} = -1$, thus $\theta = \pm j(2n-1)\pi/2$, where n is a positive integer. From this and (13) we obtain the roots of the numerator:

$$s_{zn} = -\omega_{zn}, \quad n = 1, 2, 3, \ldots \tag{14}$$

with

$$\omega_{zn} = \frac{\pi^2(2n-1)^2}{4RC} \tag{15}$$

Similarly, for the sinh factor in the denominator, we set, $\sinh\theta = (e^{\theta} - e^{-\theta})/2 = 0$ thus $e^{2\theta} = 1$, thus $\theta = \pm j\pi n$, where $n = 0, 1, 2, \ldots$. From this and (13) we obtain the corresponding roots:

$$s_{pn} = -\omega_{pn}, \quad n = 0, 1, 2 \ldots \tag{16}$$

with

$$\omega_{pn} = \frac{\pi^2 n^2}{RC} \tag{17}$$

Using these results, the cosh and sinh functions in (12) can be represented by their Weierstrass product expansions, which are known to exist for complex functions that are analytic for all values of their complex argument, and which have simple zeros [23,32,33]. These product expansions are $\cosh\theta = \prod_{n-1}^{\infty}\{1 + 4\theta^2/[(2n-1)^2\pi^2]\}$ and $\sinh\theta = \theta\prod_{n-1}^{\infty}[1 + \theta^2/n^2\pi^2]$. Using these and (13) in (12) we obtain:

$$Z_o(s) = \frac{1}{sC} \frac{\prod_{n=1}^{\infty}\left(1 + \frac{s}{\omega_{zn}}\right)}{\prod_{n=1}^{\infty}\left(1 + \frac{s}{\omega_{pn}}\right)} \tag{18}$$

The quantities s_{zn} and s_{pn} obtained earlier are, respectively, the zeros and poles of the rational expression for $Z_o(s)$ in the above equation.

At very low frequencies ($\omega \ll \omega_{z1}$), we have $Z_o(j\omega) \approx 1/(j\omega C)$, consistent with the observation of low-frequency capacitive

storage behavior made earlier. This observation will prove useful in the discussions that follow.

2.2. Truncated Weierstrass approximation

For an Nth-order approximation, the product in the denominator of the second fraction in (18) must be of order $N-1$ (note the extra pole at $s=0$ outside that product). In order to keep the important property in (11), the numerator order must be less than that of the denominator. We want to keep as many of the zeros as possible while satisfying this constraint; this leads to a numerator of order $N-1$. We thus approximate (18) by:

$$Z_o(s)=\frac{1}{sC}\frac{\prod_{n=1}^{N-1}\left(1+\frac{s}{\omega_{zn}}\right)}{\prod_{n=1}^{N-1}\left(1+\frac{s}{\omega_{pn}}\right)} \tag{19}$$

which can also be written in the form:

$$Z_o(s)=\frac{k_N}{sC}\frac{\prod_{n=1}^{N-1}(s+\omega_{zn})}{\prod_{n=1}^{N-1}(s+\omega_{pn})} \tag{20}$$

where

$$k_N=\prod_{n=1}^{N-1}\frac{\omega_{pn}}{\omega_{zn}} \tag{21}$$

The phase and magnitude of $Z_o(j\omega)$ using (19) are shown in Fig. 7a and b, for three values of the order of approximation N, and are compared to the ideal behavior from (9). It is seen that a large order is needed for accurate representation over a significant frequency range.

It is appropriate to study how the individual terms in (19) contribute to the overall behavior. This will be accomplished using the phase response. Using $s=j\omega$ in (19), it is seen that the phase starts at $-90°$ in the limit of zero frequency. As the frequency is raised, each term of the form $(1+j\omega/\omega_{zn})$ in the numerator contributes a phase change that increases from 0°, goes through +45° at $\omega=\omega_{zn}$, and asymptotically reaches +90°. Similarly, each term of the form $(1+j\omega/\omega_{pn})$ in the denominator contributes to the impedance a phase change that decreases from 0°, goes through $-45°$ at $\omega=\omega_{pn}$, and asymptotically reaches $-90°$. It is the interplay between these contributions that produces an overall value of $-45°$ in the CPE region. The beauty of the Weierstrass expansion is that it distributes the zero and pole frequencies, ω_{zn} and ω_{pn}, in such a way that the phase response is smooth and practically equal to $-45°$ if an infinite number of terms are included. If, however, $N-1$ terms are used in the products in (19), the highest-frequency pole eventually wins out, and takes the phase toward $-90°$.

The values of the zero and pole frequencies, ω_{zn} and ω_{pn}, for $N=12$, are indicated along a logarithmic frequency axis by "$\circ$" and "$\times$", respectively in the upper row of Fig. 8 (the lower row will be discussed in the next subsection). Note that the "$\circ$" and "$\times$" symbols indicate the positive frequencies corresponding to each zero and pole; the zeros and poles themselves are negative, as seen from (14) and (16). As can be checked from (15) and (17), as n is increased, the quantities $\omega_{p,n+1}/\omega_{pn}$, $\omega_{z,n+1}/\omega_{zn}$, and ω_{pn}/ω_{zn} all approach monotonically 1 in the limit. This explains the fact that, as n increases, the logarithmic distance between successive zeros, and between successive poles decreases, and the poles tend to pile up on top of the zeros, as seen along the logarithmic axis for the top row in Fig. 8. This suggests that the near-cancelation between poles and zeros, on which the Weierstrass product relies, will require many more poles and zeros for a significant logarithmic increase of the frequency range of validity.

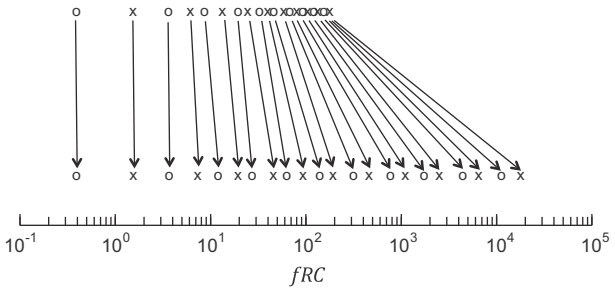

Fig. 8. Mapping involved in stretching pole and zero frequencies.

2.3. A "stretched constellation" approach

The unmodified, truncated Weierstrass approximation used above provides low error for low frequencies but unacceptable error once the frequency is somewhat raised (Fig. 7). An increase of the frequency range of validity can be achieved if one is willing to accept a very small error in the transition region. This increase of the range of validity can be accomplished by spreading the poles and zeros apart, as shown at the bottom row in Fig. 8, resulting in what we call the "stretched pole-zero constellation". By spreading apart the poles and zeros, their opposing effects on the phase at intermediate frequencies will not cancel out completely, but as long as they are relatively close to each other, the error incurred can be expected to be small.

Let ω_i be any pole or zero frequency. We define a new set of poles and zeros $\{\hat{\omega}_i\}$ as follows:

$$\hat{\omega}_i=r_i\omega_i \tag{22}$$

where r_i is the "stretching factor" corresponding to pole or zero frequency ω_i. The above relation defines a mapping between the sets $\{\omega_i\}$ and $\{\hat{\omega}_i\}$, indicated by the arrows in Fig. 8. The upper row indicates the frequency positions of the original pole and zero frequencies; the bottom row indicates their position in the stretched pole-zero constellation.

The problem now is how to choose the values of the stretching factors r_i. A clue on how to do this comes from Bode plot theory, where a logarithmic frequency axis is used. It is known that phase and magnitude contributions and errors depend not on absolute frequency numbers, but rather on frequency ratios. Thus, for example, we know [34] that the phase contributed by a zero at frequency ω_z becomes 84.3° a decade above ω_z, where "decade" means a frequency ratio of 10. Frequency decades represent equal distances along a logarithmic axis, such as the one used in Fig. 8. This intuitively suggests that a reasonable candidate for the stretching factors would be one that makes their logarithm proportional to the frequency they are stretching. This implies stretching factors of the form:

$$r_i=10^{\frac{\omega_i}{\omega_0}} \tag{23}$$

where $1/\omega_0$ is a scaling factor.

To set the value of ω_0, let us assume that we want the maximum pole frequency, $\omega_{p,N-1}$, to be stretched by ξ; in other words:

$$\xi=\frac{\hat{\omega}_{p,N-1}}{\omega_{p,N-1}} \tag{24}$$

From the above three equations we find $\omega_0=\omega_{p,N-1}/\log_{10}\xi$. Using this in (23), we obtain a formula for the stretching factors:

$$r_i=\xi^{\frac{\omega_i}{\omega_{p,N-1}}} \tag{25}$$

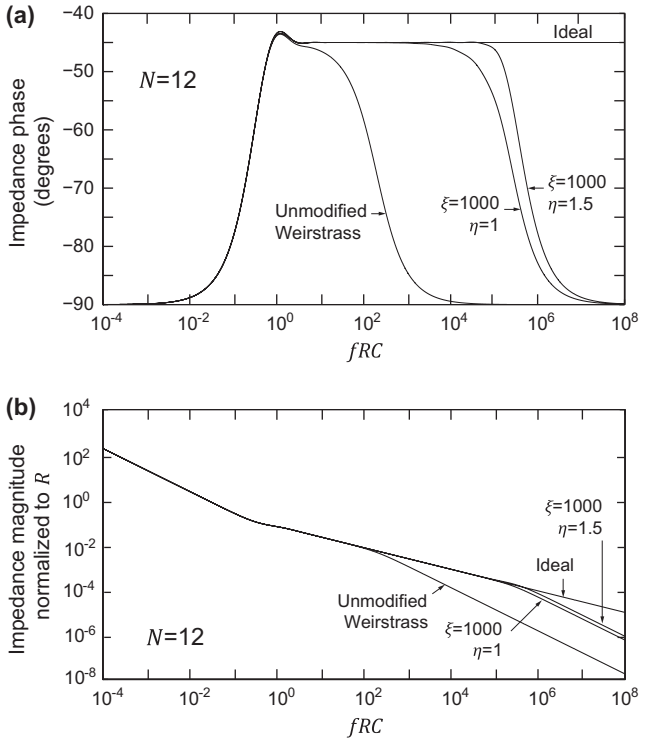

Fig. 9. Effect of η on (a) phase and (b) magnitude.

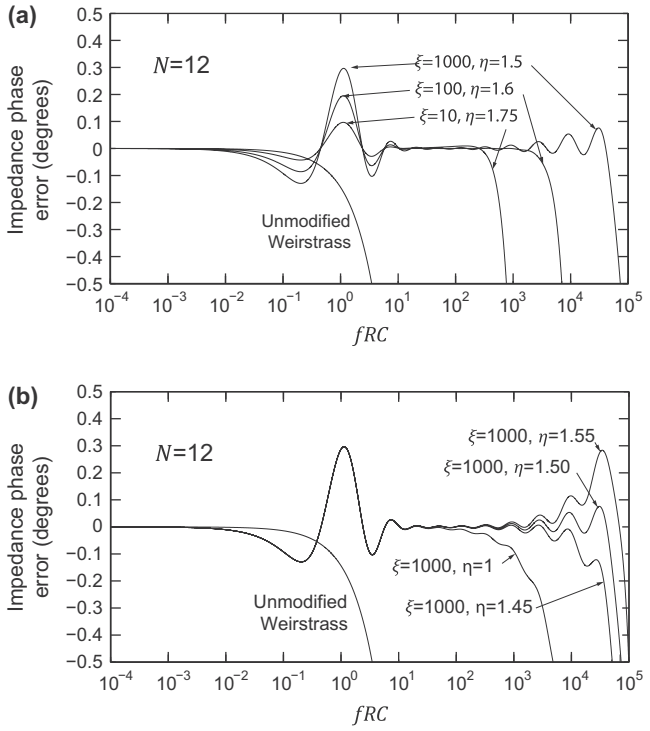

Fig. 10. (a) Effect of ξ and (b) effect of η on phase error. In (a), η is slightly adjusted for each curve, to optimize high-frequency behavior.

We can further optimize things by increasing the last pole frequency found as above by a factor η, to partially compensate for the missing higher-order terms in the product. Thus, we replace the highest pole frequency found above, $\hat{\omega}_{p,N-1}$, by:

$$\hat{\hat{\omega}}_{p,N-1} = \eta \hat{\omega}_{p,N-1} \tag{26}$$

Consequently, the constellation stretching procedure consists of the following steps. We choose a value for ξ, the stretching factor of the highest pole frequency; we use this to find the stretching factors of the other poles and zeros from (25); finally, we further stretch the resulting highest-frequency pole by a factor η, using (26). Reasonable choices for the values of ξ and η are discussed below in terms of examples. In the numerical examples below, $N = 12$ unless stated otherwise.

Fig. 9a shows the phase for a stretching factor ξ of 1000, and for two values of η. The unstretched (original) truncated Weierstrass is also shown as a reference. Over two orders of magnitude of improvement is seen. Fig. 9b shows the corresponding magnitude plots.

Fig. 10 shows the phase error with respect to the ideal response obtained from (9). Fig. 10a illustrates the effect of ξ. For a given N, the larger ξ is, the larger the frequency range of validity will be, but a larger phase error must be tolerated near the transition frequency from capacitive to CPE behavior. The value of η has been adjusted to provide a relatively flat band near the upper frequency limit of validity. Fig. 10b shows the effect of η on the phase error, for $\xi = 1000$. It is seen that the phase error near the transition point to CPE behavior is about 0.3°. From this figure, the role of η can be clearly seen; it is to adjust the peaking of the frequency response near the end of its range of validity. If, at that end, a 0.3° error (same as at the transition point) can be tolerated, the frequency response can be extended, as shown by the curve for $\eta = 1.55$; otherwise, this error peaking can be reduced using $\eta = 1.50$. Such adjustments are very easy to perform by trying a few values and observing their effect on the error plots.

The effects of ξ and η on the magnitude error are similar to those discussed above, although the values of η needed to eliminate the peaking near the upper frequency limit of validity are a little different from those in Fig. 10b. However, at such frequencies the magnitude itself is extremely small, and thus such details are unlikely to be important.

Fig. 11 shows what happens assuming that the desired upper frequency limit of validity is fixed. As seen, if a high order is allowed (24th), the maximum phase error near the capacitive-to-CPE transition can be made very small (less than 0.05°). However, even with 12th order, this error does not become excessive (about 0.2°).

Up to this point, the emphasis has been on a very wide frequency range of validity (several orders of magnitude above the transition region). However, as already mentioned, at very high frequencies the magnitude of the impedance becomes negligible and in a real system such as a battery cell, other phenomena become prevalent. For this reason, often the needed upper limit of validity of a model is limited. In such cases, and depending on the phase

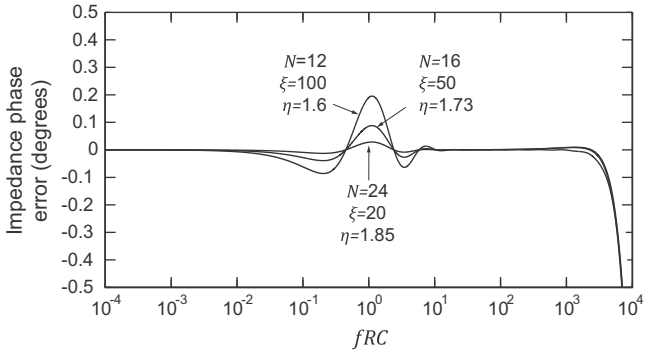

Fig. 11. Comparing different orders, with the same upper limit of validity.

error that can be accepted, the needed model order can be significantly reduced. For example, with the upper frequency limit of validity taken to be 80 times the transition point if a phase error of 0.3° can be accepted, a 6th-order model will suffice, thanks to the stretched constellation approach. A low order model implies efficiency and speed in a simulation environment, making the method suitable for use in "real time" simulations.

It can be seen from several figures above that the stretching law in (25) works well, with the larger error being near the point $fRC = 1$. This suggests that, if this error is to be minimized, more attention needs to be paid around this point. The behavior in that vicinity is governed by the low-frequency poles and zeros. Thus, one can consider leaving the first few original pole and zero frequencies intact, or at least stretch them less drastically than suggested by (25). To accomplish this, one would use a stretching law that starts at value 1, staying relatively constant for the first few poles and zeros, and then gradually transitioning to the stretching factors in (25). While such an empirical function for the stretching law can be found, it is not considered worthwhile doing so, as it would complicate the formulation, and we have already reached the point of diminishing returns, given that the phase error in the transition point is small anyway.

3. Equivalent circuit

Classical circuit synthesis [23,26,29,31] can be used to synthesize an equivalent circuit with a ladder structure. The procedure is as follows. After multiplications are carried out in (20), the admittance $Y_o(s) = 1/Z_o(s)$ is of the form of a ratio of two polynomials, $P_N(s)/Q_{N-1}(s)$, where the subscripts denote the degree of the two polynomials. Polynomial division is then performed, resulting in a quotient of the form sC_o, where C_o is the ratio of the two leading coefficients of the polynomials and, for the type of polynomials we are dealing with, a remainder of order $N-1$, denoted by $P_{N-1}(s)$, thus leading to $Y_o(s) = sC_o + P_{N-1}(s)/Q_{N-1}(s)$. We write this as $sC_o + 1/[Q_{N-1}(s)/P_{N-1}(s)]$. Performing the division indicated in the last quantity, we obtain a constant term, denoted by R_1, and a quotient of order $N-2$; we continue in this fashion, each time performing polynomial division and writing the resulting quotient-over-divisor fraction as 1 over its inverse. This leads to an expression of the form:

$$Y_o(s) = sC_0 + \cfrac{1}{R_1 + \cfrac{1}{sC_1 + \cfrac{1}{R_2 + \cfrac{1}{sC_3 + \ldots}}}} \tag{27}$$

By inspection, this is the input admittance of the ladder circuit in Fig. 4, where each element corresponds to a quotient in the repeated division process outlined above.

From the above procedure, involving (20) we conclude:

$$C_0 = \frac{C}{k_N} \tag{28}$$

Performing the above procedure on a 12th order stretched constellation approximation, and assuming $R = 1\ \Omega$, $C = 1$ F, $\xi = 1000$, and $\eta = 1.50$, we obtain the element values shown in Fig. 12. The resulting frequency response is shown in Fig. 13, and is compared to the response of a 5001th-order equal-R, equal-C ladder. The upper frequency limit of validity is at least an order of magnitude higher for the circuit of Fig. 12.

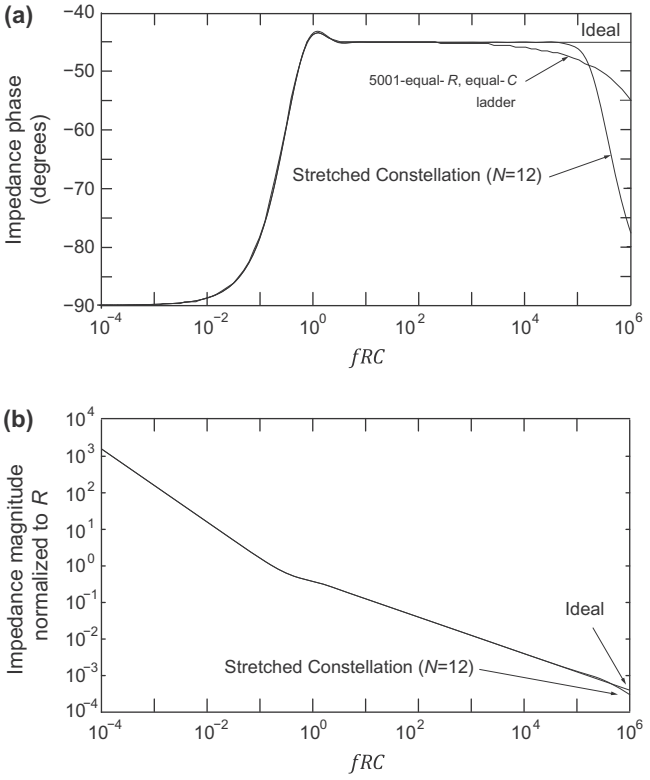

Fig. 13. Simulated impedance of the ladder in Fig. 12, compared to the exact impedance of the structure in Fig. 1 and of a 5001th-order equal-R, equal-C ladder. (a) Phase and (b) magnitude. $N = 12$, $R = 1\ \Omega$, $C = 1$ F, $\xi = 1000$, $\eta = 1.50$.

4. Simulation of internal behavior

The stretched-constellation ladder was developed for modeling correctly the impedance across the input terminals. It is consistent with the idea in Fig. 5 (note that the resistances and capacitances in Fig. 12 get progressively larger, as we go toward the right), and can successfully model even the *internal* behavior in the distributed structure. This is illustrated in Fig. 14, which compares the transient response of the stretched-constellation ladder of Fig. 12 to that of a 5001th-order equal-R, equal-C ladder. The capacitances of both ladders are "charged" to 1 V, and then an input is applied, consisting of a 0.8 A discharging current for 1 s, followed by a 0.6 A charging current. In Fig. 14a, the voltages across the capacitors in Fig. 12 are shown; Fig. 14b shows the voltages at the corresponding points in the 5001th-order equal-R, equal-C ladder, taken as the points where the total capacitance from the input to those points is the same in the two circuits. It can be seen that the responses for the two circuits closely match, and that the 12th-order stretched-constellation ladder successfully models

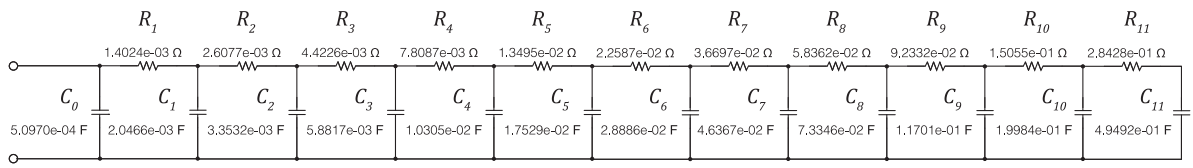

Fig. 12. 12th Order RC ladder circuit designed for $\xi = 1000$ and $\eta = 1.50$. $R = 1\ \Omega$, $C = 1$ F.

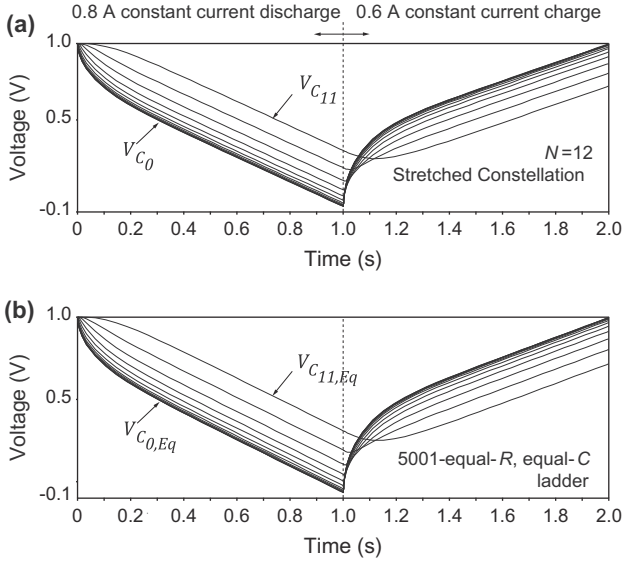

Fig. 14. (a) Response of the ladder in Fig. 12 to a current pulse, consisting of a 0.8 A discharging current for 1 s, followed by a 0.6 A discharging current. The voltages across the capacitors are shown. (b) Corresponding response of a 5001th-order equal-*R*, equal-*C* ladder circuit (Fig. 3a). Corresponding points are selected so that the total capacitance from the input to those points is the same as that in the ladder of Fig. 12.

the propagation of the input disturbance to internal points. Various phenomena can be studied thanks to this. For example, it can be observed that after the input current changes direction, capacitors toward the right side of the ladder keep discharging for some time, reflecting the dynamics of diffusion. This happens because the input disturbance does not immediately affect such faraway points.

The computation time needed for the stretched-constellation ladder was found to be 1953 times shorter than for the 5001th-order one. No price seems to be paid for such drastic computational savings; in fact, the 12th-order stretched-constellation ladder can successfully model the input impedance over a significantly larger frequency range, as has been shown in Fig. 13.

5. Capacitances and storage

The presence of C_0 in the ladder circuit of Fig. 4 is instrumental, as this is the element that ensures that the magnitude of the impedance asymptotically goes to 0 as the frequency is increased, in accordance with (11). This capacitance would not be present if the numerator of (19) had been chosen to be of order *N*.

For the total capacitance in the ladder circuit of Fig. 4 we have

$$\sum_{n=0}^{N-1} C_n = C \tag{29}$$

where *C* is the total capacitance in the distributed-parameter element in Fig. 1b . This can be confirmed by inspection of the ladder circuit in Fig. 4. At very low frequencies the voltages across the resistors are negligible compared to those across the capacitors. As a consequence, all capacitors are effectively in parallel, resulting in a total capacitance *C* as expected from (18). This, in the circuit of Fig. 4, corresponds to the case in an actual diffusion layer, where the frequency is so low that the concentrations involved have time to reach equilibrium throughout the structure, i.e. the structure operates quasi-statically. The total resistance in the ladder circuit is of similar magnitude as the total resistance in the structure of Fig. 1b. The two are not exactly equal. This is a trivial difference: the two can be made equal, simply by adding a small resistance

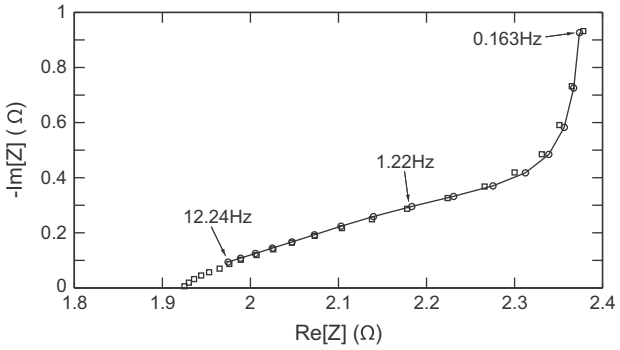

Fig. 15. Nyquist plot. Squares: measurements on a supercapacitor [35], circles: 6th-order model with $R = 0.00152\ \Omega$, $C = 1120$ F, $\xi = 4$, and $\eta = 1.7$, with real part offset by a constant equal to $0.00188\ \Omega$ (see text).

with one end floating, at the right end of the ladder; such a resistance would not carry a current, and would not alter the impedance $Z_o(s)$.

The fact that the low-frequency behavior is capacitive (corresponding to the factor $1/sC$ in (19)), allows one to use it to predict storage in battery models. It is acknowledged, however, that other phenomena have to be taken into account in a complete battery model [3]. There are enough degrees of freedom here: *C* in (19) can be chosen as the storage capacity, and then the rest of the elements can be chosen for the correct frequency behavior, as discussed in Section 2. In fact, once an equivalent circuit for a given *N* has been designed, it can be adopted to other cases by using the procedures known as magnitude scaling, impedance scaling, and frequency scaling [34] as appropriate.

6. Comparison to experimental data

The diffusion impedance of electrochemical devices satisfying (3) can be modeled by the electrical impedance in (9) (see, for example, [3,11]); thus, the above results can profitably be used. The accurate prediction of magnitude and phase throughout the range of validity of the ladder circuit based on the stretched constellation approximation, results in accurate prediction of the real and imaginary parts of the impedance. This then leads to accurate Nyquist plots, which are widely used in impedance spectroscopy [3]. An example is shown in Fig. 15. The squares are measurements on a supercapacitor [35]. The circles, which correspond to logarithmic frequency spacing, are from a 6th-order model, with $\xi = 4$ and $\eta = 1.7$, with the real part shifted by $0.00188\ \Omega$ to account for series resistance, not present in the model. It was found that the values of ξ and η were not critical at all, since they chiefly affect the very high frequency region, in which other effects become dominant. Such effects dominate frequencies above 12 Hz, and cannot be described by the diffusion equation; thus, no fitting was attempted at such frequencies. It is important to note that, as seen in Fig. 15, the approach we have presented successfully models the structure in the CPE region, the capacitive (storage) region, and the transition region in-between.

7. A comment on average power

It is desirable that an equivalent circuit for $Z_o(s)$ predict accurately the (real) average power dissipated in it, as this represents losses in the system. In sinusoidal steady state, assuming the impedance is driven by a current of *rms* value I_{rms}, this power is given by:

$$P = I_{rms}^2 Re[Z_o(j\omega)] \tag{30}$$

where $Re[Z_o(j\omega)]$ represents the real part of the impedance. From this and the accuracy of predicting the magnitude and phase of the impedance and thus its real part, it can be seen that the power dissipated in the impedance can be predicted accurately throughout the range of validity of the above approximations.

8. Conclusions

We have pointed out several unique advantages of the non-uniform *RC* ladder as an equivalent circuit for modeling one-dimensional diffusion. These advantages include the ability to correctly model storage, the ability to correctly model behavior at internal points, and computational efficiency. We have presented systematic, analytical ways for finding approximations for the poles and zeros of expressions that model the electrochemical impedance of structures with finite length (referred to sometimes as "finite-length Warburg impedance"), with a blocking boundary condition. A stretched constellation technique has been utilized for this purpose, therefore making it possible to use low-order circuits that match electrochemical impedance over a wide frequency range. Circuit simulations were used to confirm the theory. The results in this paper make possible the computationally efficient modeling of the electrochemical impedance with conventional, lumped-element circuits, suitable for use in conventional circuit simulators.

Acknowledgments

The authors would like to thank Dr. Kun Zhang for his help in producing simulation results.

References

[1] E. Warburg, Ann. Phys. Chem. 67 (1899) 493–499.
[2] R. De Levie, Electrochim. Acta 9 (1964) 1231–1245.
[3] E. Barsoukov, J.R. Macdonald, Impedance Spectroscopy – Theory, Experiment, and Applications, Wiley-Interscience, New Jersey, 2005.
[4] D.R. Franceschetti, J.R. Macdonald, J. Electroanal. Chem. 101 (1979) 307–316.
[5] C. Ho, I.D. Raistrick, R.A. Huggins, J. Electrochem. Soc. 127 (February) (1980) 343–350.
[6] R.D. Armstrong, J. Electroanal. Chem. 198 (1986) 177–180.
[7] E. Kuhn, C. Forgez, P. Laognotte, G. Friedrich, J. Power Sources 158 (2006) 1490–1497.
[8] J.R. Scully, D.C. Silverman, M.W. Kendig, Electrochemical Impedance: Analysis and Interpretation, ASTM Special Technical Publication 1188, Fredericksburg, 1993.
[9] R.P. Buck, C. Mundt, Electrochim. Acta 44 (12) (Jan. 1999) 1999–2118.
[10] B.E. Conway, Electrochemical Capacitors – Scientific Fundamentals and Technological Applications, Kluwer Academic/Plenum Publishers, New York, 1999.
[11] J. Bisquert, G. Garcia-Belmonte, F. Fabregat-Santiago, P.R. Bueno, J. Electroanal. Chem. 475 (2) (1999) 152–163.
[12] J. Bisquert, A. Compte, J. Electroanal. Chem. 499 (1) (2001) 112–120.
[13] S. Buller, M. Thele, R.W.A.A. De Doncker, E. Karden, IEEE Trans. Indust. Appl. 41 (3) (2005) 742–747.
[14] E. Kuhn, C. Forgez, P. Laognotte, G. Friedrich, J. Power Sources 158 (2006) 1490–1497.
[15] P. Agarwal, M.E. Orazem, J. Electrochem. Soc. 139 (7) (1992) 1917–1927.
[16] D. Andre, M. Meiler, K. Steiner, H. Walz, T. Soczka-Guth, D.U. Sauer, J. Power Sources 196 (2011) 5349–5356.
[17] T.K. Dong, A. Kirchev, F. Mattera, J. Kowal, Y. Bultel, J. Electrochem. Soc. 158 (3) (2011) A326–A336.
[18] P.L. Moss, G. Au, J.P. Zheng, E.J. Plichta, J. Electrochem. Soc. 155 (2008) A986–A994.
[19] J. Valsa, J. Vlach, Int. J. Circuit Theory Appl., doi:10.1002/cta.785.
[20] P.L. Moss, J.P. Zheng, G. Au, P.J. Cygan, E.J. Plichta, J. Electrochem. Soc. 154 (2007) A1020–A1025.
[21] J.R. Macdonald, LEVM software, <http://www.jrossmacdonald.com>.
[22] J. Miller, in: S.P. Wolsky, N. Marincic (Eds.), Proc. Second International Symposium on Electrochemical Capacitors and Similar Energy Storage Devices, Florida Educational Seminars, Boca Raton, FL, December 7–9, 1992.
[23] M.S. Ghausi, J.J. Kelly, Introduction to Distributed-Parameter Networks, Holt, Rinehart, and Winston, New York, 1968.
[24] L.W. Nagel, D.O. Pederson, SPICE (Simulation Program with Integrated Circuit Emphasis, Memorandum no. ERL-M382, University of California, Berkeley, April 1973.
[25] <http://www.cadence.com/products/pcb/spice/pages/default.aspx>, (accessed 08.01.13).
[26] E.A. Guillemin, Synthesis of Passive Networks, John Wiley, New York, 1957.
[27] B. Hirschorn, M.E. Orazem, B. Tribollet, V. Vivier, I. Frateur, M. Musiani, Electrochim. Acta 55 (2010) 6218–6227.
[28] W.G. Pell, B.E. Conway, W.A. Adams, J. de Oliveira, J. Power Sources 80 (1999) 134–141.
[29] S.C. Dutta-Roy, B.A. Shenoi, J. Franklin Inst. 282 (5) (1966) 318–329.
[30] J. Bisquert, G. Garcia-Belmonte, P.R. Bueno, E. Longo, L.O.S. Bulhões, J. Electroanal. Chem. 452 (1998) 229–234.
[31] S.C. Dutta Roy, IEEE Trans. Circuit Theory CT-14 (3) (1967) 264–274.
[32] M.R. Spiegel, Complex Variables, McGraw-Hill, 1964.
[33] M. Abramowitz, I.A. Stegun (Eds.), Handbook of Mathematical Functions with Formulas, Graphs, and Mathematical Tables, National Bureau of Standards, Applied Mathematics Series, 1964.
[34] M. Van Valkenburg, Analog Filter Design, Oxford University Press, 1995.
[35] S. Buller, Impedance-based simulation models for energy storage in advanced automobile power systems, Dissertation, RWTH Aachen University, 2003.